Marco Salviato[1]
Research Assistant Professor
Civil and Environmental Engineering,
Northwestern University,
Evanston, IL 60208

Viet T. Chau
Civil and Environmental Engineering,
Northwestern University,
2145 Sheridan Road,
Evanston, IL 60208

Weixin Li
Civil and Environmental Engineering,
Northwestern University,
2145 Sheridan Road,
Evanston, IL 60208

Zdeněk P. Bažant[2]
McCormick Institute Professor and
W.P. Murphy Professor
Civil and Mechanical Engineering and
Materials Science,
Department of Civil and
Environmental Engineering,
Northwestern University,
2145 Sheridan Road, CEE/A135,
Evanston, IL 60208
e-mail: z-bazant@northwestern.edu

Gianluca Cusatis
Associate Professor
Civil and Environmental Engineering,
Northwestern University,
2145 Sheridan Road,
Evanston, IL 60208
e-mail: g-cusatis@northwestern.edu

Direct Testing of Gradual Postpeak Softening of Fracture Specimens of Fiber Composites Stabilized by Enhanced Grip Stiffness and Mass

Static and dynamic analysis of the fracture tests of fiber composites in hydraulically servo-controlled testing machines currently in use shows that their grips are much too soft and light for observing the postpeak softening. Based on static analysis based on the second law of thermodynamics, confirmed by dynamic analysis of the test setup as an open system, far stiffer and heavier grips are proposed. Tests of compact-tension fracture specimens of woven carbon-epoxy laminates prove this theoretical conclusion. Sufficiently, stiff grips allow observation of a stable postpeak softening, even under load-point displacement control. Dynamic analysis of the test setup as a closed system with proportional-integrative-differential (PID)-controlled input further indicates that the controllability of postpeak softening under crack-mouth opening displacement (CMOD) control is improved not only by increasing the grip stiffness but also by increasing the grip mass. The fracture energy deduced from the area under the measured complete load-deflection curve with stable postpeak is shown to agree with the fracture energy deduced from the size effect tests of the same composite, but the size effect tests also provide the material characteristic length of quasibrittle (or cohesive) fracture mechanics. Previous suspicions of dynamic snapback in the testing of stiff specimens of composites are dispelled. Finally, the results show the stress- or strain-based failure criteria for fiber composites to be incorrect, and fracture mechanics, of the quasibrittle type, to be perfectly applicable. [DOI: 10.1115/1.4034312]

Introduction

The material failure criteria for fiber-polymer composites have for a long time been expressed in terms of stresses or strains. Examples are the maximum stress, maximum strain, deviatoric strain energy, and tensor polynomial criteria [1] sanctioned by a worldwide comparison exercise [2–4]. Their general applicability, however, is an in-grained antiquated myth, surviving from precomputer age. Such criteria apply to plastic materials, which exhibit no strain localization instability, no spurious mesh sensitivity, no material characteristic length, and no deterministic size effect.

In reality, fiber composites are quasibrittle materials (which also include concrete—as the archetypical case, tough ceramics, rocks, sea ice, rigid foams, bone, etc.). All quasibrittle materials fail by localization of softening damage into a discrete fracture. In contrast to plasticity, they exhibit a material characteristic length. This inevitably leads to a strong energetic (or nonstatistical) size effect when geometrically similar structures of different sizes are compared (e.g., see Refs. [5–10]). On sufficiently small scale, all brittle materials behave as quasibrittle.

Two basic types of size effect must be distinguished. Here the focus is on the Type 2 size effect, which occurs when a large notch or stress-free crack exists at maximum load. This size effect is weak for small specimens not much larger than the periodicity of the weave or the size of the representative volume element (RVE), for which it may seem that the stress or strain failure criteria work. But with increasing structure size, there is a gradual transition to the strong size effect of fracture mechanics caused by stored energy release associated with stress redistribution during damage. It may be noted that the Type 1 size effect occurs in structures that fail right at the initiations of a macro-crack from a damaged RVE at a smooth surface in unnotched specimens, and represents a combination of deterministic and statistical (or Weibull) size effects (omission of the deterministic aspect led to an erroneous conclusion (e.g., see Ref. [11]), namely that the Weibull modulus was a geometry-dependent variable rather than a material constant).

At mesh refinement, the use of stress or strain criteria inevitably causes a loss of objectivity, spurious mesh sensitivity, and convergence problems [9,12]. For this reason, as well as fundamentally, realistic failure analysis must be based on quasibrittle fracture mechanics, which evolved, since its dawn in the mid 1970s, into a mature and widely accepted theory. Fracture mechanics is well accepted for delamination fracture of layered two-dimensional (unstitched) fiber-composite laminates. There is even an ASTM test to determine the corresponding fracture energy [13] (although this test has just been shown to require a significant correction for transitional size effect [14].

The fact that quasibrittle fracture mechanics must apply to in-plane or flexural loading of fiber composite laminates was

[1]Present address: Assistant Professor, William E. Boeing Department of Aeronautics and Astronautics, University of Washington, Seattle, WA 98195.
[2]Corresponding author.
Contributed by the Applied Mechanics Division of ASME for publication in the Journal of Applied Mechanics. Manuscript received July 18, 2016; final manuscript received July 22, 2016; published online August 24, 2016. Editor: Yonggang Huang.

demonstrated by the numerous size effect tests performed, beginning in 1996 [10,15–18], on geometrically similar notched specimens. However, to many engineers and researchers, the size effect tests have been unconvincing, for two reasons: (1) some of them erroneously considered the size effect to be statistical, due to material randomness (although this is possible only for Type 1 failures); (2) others rejected the cohesive crack model because a gradual postpeak softening could never be observed in experiments. The specimens always failed explosively right after attaining the maximum load, and the load applied by the testing machine dropped suddenly to zero. The sudden drop seemed to indicate a linear elastic fracture mechanics (LEFM) behavior, but the LEFM clearly did not fit test data, and also suggested a snapback, but the area under the snapback curve would give a much smaller fracture energy than the LEFM testing.

In this paper (the basic idea of which has been documented on July 4, 2016, in arXiv submission [19]), it is shown that the foregoing objection is invalid, that postpeak can be measured, in a stable test, and that quasibrittle fracture mechanics with transitional size effect is perfectly applicable to fiber-polymer composites.

Highly Stiff Test Frame With Fast Servo Control Via CMOD

A similar history occurred long ago for concrete and rock. Until the 1960s, it was believed that concrete and rock explode at maximum load and the load applied by the testing machine drops suddenly to zero. Then, beginning in 1963, several researchers, including Hughes, Chapman, Hillsdorf, Rüsch, Evans, and Marathe [20–23] came up with the idea of using, for both tensile and compressive tests of concrete, a much stiffer loading frame and fast hydraulic servo control. Suddenly, a gradual postpeak decline of the compressive or tensile load could be observed. Similar efforts to stabilize postpeak in compression testing of rock were made, beginning 1963, by Neville G.W. Cook and Charles Fairhurst at University of Minnesota, Minneapolis, MN [24–26]. The stability of postpeak was further enhanced by controlling the test electronically with a gage measuring the crack-mouth opening displacement (CMOD). A servo-controlled stiff machine of MTS Corporation was built in 1967.

This discovery opened a revolution in the mechanics of concrete and rock, and was one essential factor that prompted the development of quasibrittle fracture mechanics. The stabilizing effect of machine stiffness was mathematically demonstrated by static stability analysis in Ref. [12], which led to an equation for the required machine stiffness as a function of the maximum steepness of the postpeak load-deflection curve (see also Refs. [6–8]).

Unfortunately, the same measures did not work for fiber composites. The same stiff frames with fast servo control did not suffice. The CMOD control of notched compact tension specimens and of edge-notched strips was tried at Northwestern, but did not work. Neither did the control of crack tip opening displacement (CTOD). The reason will be clarified here.

Static Criterion of Stability

For the purpose of static analysis, the test system can be considered as the coupling of two elements: (1) the testing machine frame of stiffness K_m with the specimen grips (or fixtures) of stiffness K_g form one elastic element of stiffness K_m, and (2) the test specimen, of tangential (or incremental) stiffness K_s is the second element. Figure 1 shows a schematic of the testing frame.

Based on the second law of thermodynamics, the test setup becomes unstable if there exists a perturbing load that produces negative work ΔW on the test setup, thus causing an increase of entropy, ΔS (in detail, see Refs. [6–8], Chap. 10). So, we imagine a perturbing load δP to be applied axially at the load point of the test specimen while the system is in equilibrium. The combined

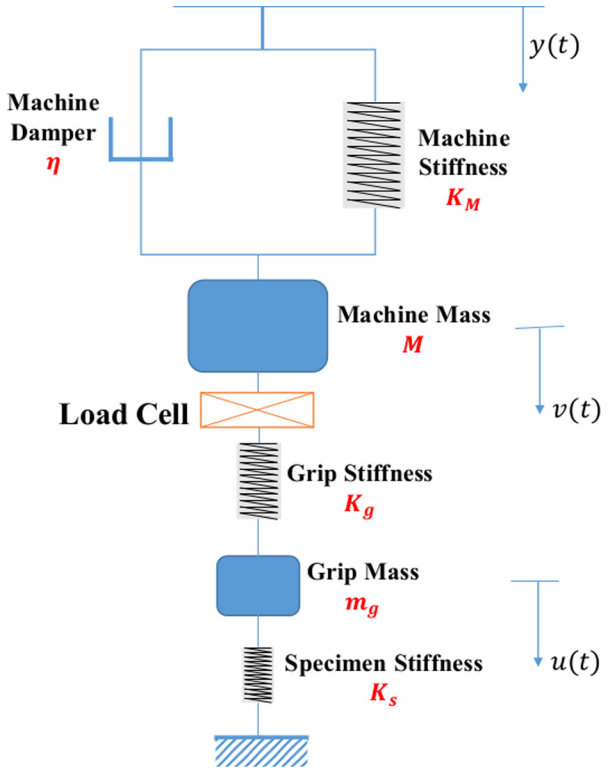

Fig. 1 Simplified schematic of a universal servo-hydraulic testing machine

stiffness of the machine with the grips is $K_{mg} = 1/(1/K_m + 1/K_g)$ and the total stiffness K_t resisting δP is $K_{mg} + K_s$. The displacement under δP in the direction of δP is $\delta v = \delta P/K_t$, and

$$\Delta W = -T\,\Delta S = \frac{1}{2}\,\delta P\,\delta v = \frac{1}{2}\,K_t\,(\delta v)^2 \tag{1}$$

where T = absolute temperature. The equilibrium of the system is stable if and only if $\Delta W > 0$, which requires that $K_t > 0$ or

$$K_t = \frac{1}{1/K_m + 1/K_g} + K_s > 0 \tag{2}$$

Consider now a typical 20 ton testing machine (e.g., MTS) used in the testing of composites and a typical compact tension specimen consisting of 24 layers of woven carbon fiber epoxy

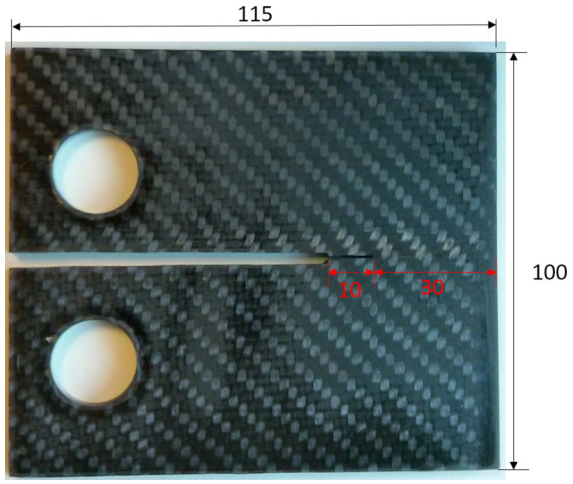

Fig. 2 Dimensions of 2D woven composite specimens

composites for a total thickness of 5.4 mm (see Fig. 2). The typical characteristics are:

- Machine frame stiffness: $K_m = 260$ MN/m.
- Stiffness of standard specimen grips: $K_g = 0.768$ MN/m.
- The steepest slope of the measured postpeak load-deflection curve of the test specimen: $K_s = -0.830$ MN/m.
- Mass of machine frame: $m_m = 500$ kg.
- Mass of grips (or fixture): $m_g = 0.919$ kg.
- Characteristic halftime of machine hydraulics delay: $\tau = 0.02$ s (defined as the time to approach halfway to a suddenly changed setting of electronic control).

Using these values, we find from Eq. (2) that

$$K_t = -0.06426 \text{ MN/m} < 0 \quad \text{... unstable} \tag{3}$$

i.e., the tested specimen is unstable. This agrees with the common wisdom of the last 50 years—it is impossible to observe gradual postpeak softening in tensile tests of fiber composites. But is it, really?

The grip stiffness is an aspect that has so far eluded attention. It has generally been assumed that the standard grips provided by the manufacturers are stiff enough. But comparison of K_g with K_m suggests otherwise. It was, therefore, decided to produce special massive grips (Fig. 3), with the following stiffness and mass;

- $\tilde{K}_g = 192.4$ MN/m (=74% K_m).
- $\tilde{m}_g = 9.419$ kg (=10 m_g).

Compared to the current standard grips, they are about ten times heavier and 250 times stiffer. Equation (2) gives

$$K_t = 109.6 \text{ MN/m} > 0 \quad \text{... stable} \tag{4}$$

Eureka—stability is achieved!

Using these grips, the composite compact tension specimens (Fig. 3) exhibited stable progressive softening, and not only under CMOD control but also under load-point control. The grips overcame the puzzling feature that the fracture energy G_f deduced from the size effect tests was much larger than the maximum possible area under a snapback curve. In fact, the area indicated by G_f required a rather gradual progressive softening, and this is what is now observed with the new grips.

From Eq. (2), one can obtain the minimum grip stiffness, necessary for stability, based on the estimated steepest postpeak slope K_s

$$[K_g]_{\min} = \frac{1}{1/|K_s|_{\max} - 1/K_m} \quad (K_s < 0) \tag{5}$$

Test Stabilization by CMOD or CTOD Control

The usual way to stabilize postpeak softening is to control the Crack Mouth (or Crack Tip) Opening Displacement (CMOD or CTOD). Let w be the relative displacement across the crack mouth or across the crack-tip region. Then, let us denote as F a fictitious force working on w although in reality F=0. The incremental (or tangential) cross compliance C_{sc} between the load P and displacement w is derived by considering the relations

$$\mathrm{d}u = C_s \mathrm{d}P + C_{sc}\mathrm{d}F \tag{6}$$

$$\mathrm{d}w = C_{sc}\mathrm{d}P + C_{cc}\mathrm{d}F \tag{7}$$

where P = applied force and $C_s = 1/K_s$ = direct (load-point) incremental (or tangential) compliance of the specimen. According to the LEFM (e.g., see Ref. [9])

$$C_{sc} = \frac{2}{bDE'}\int_0^{\alpha} k(\alpha')k_c(\alpha')\mathrm{d}\alpha' \tag{8}$$

where $\alpha = a/D$, a = crack length, D, b = specimen dimension (or size) and width; $k(\alpha), k_c(\alpha)$ = dimensionless stress intensity factors due to applied load P and to fictitious load F; $k = K_I b\sqrt{D}/P$ where K_I = actual stress intensity factor; for plane stress $E' = E$ = Young's modulus, and for plane strain $E' = E/(1-\nu^2)$ where ν = Poisson ratio. Because $F = 0$, Eqs. (6) and (7) reduce to $\mathrm{d}u = C_s\mathrm{d}P$ and $\mathrm{d}w = C_{sc}\mathrm{d}P$ or

$$\mathrm{d}u = r_{sc}\,\mathrm{d}w, \quad r_{sc} = \frac{C_s}{C_{sc}} \tag{9}$$

The same equations apply to CTOD control, if w is redefined as the crack tip opening displacement.

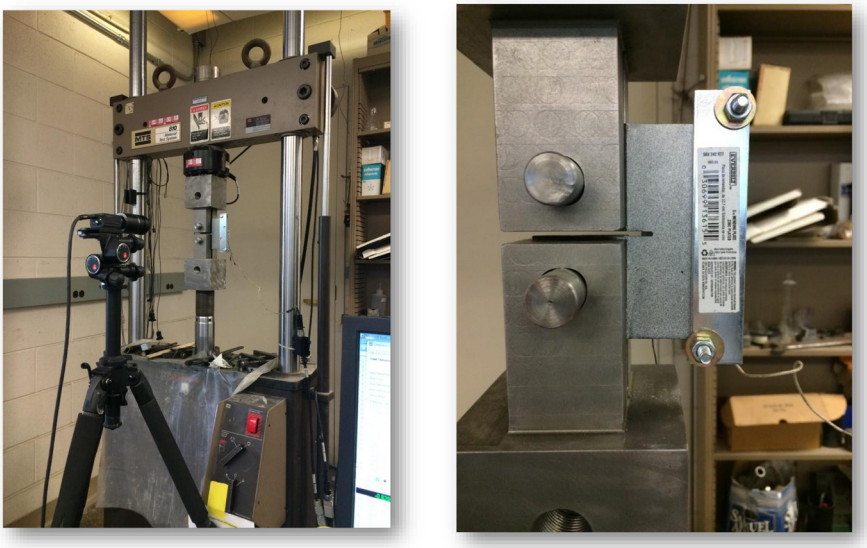

Fig. 3 (*a*) Experimental setup considered in the analysis and (*b*) new massive grips designed to achieve stable postpeak

The advantage of using CMOD or CTOD control is that, during the fracture test, w always increases. So, by controlling w, the postpeak softening can be measured even if the specimen is unstable under load-point control. But there is a caveat—the response of testing machine with its hydraulics must be fast enough. For notched concrete and rock specimens tested in the servo-controlled stiff machines introduced since 1963, it has been fast enough. But for strong and very light specimens, such as those of woven laminates, it has obviously not been fast enough, since all the attempts to measure the postpeak by means of CMOD of CTOD control have failed. To explain, we turn to dynamic analysis of stability (as thermodynamics applies only at, or very near, equilibrium.

Using Mass to Make Hydraulics Response Delay Tolerable

For half a century, the impossibility to obtain a stable postpeak softening under CMOD or CTOD control has been blamed on some unspecified peculiar property of composites. However, the present discovery of stable postpeak with very stiff grips shows that there is nothing peculiar in the material behavior of composites. So the only possible explanation why CMOD alone cannot control the postpeak test is that the response of hydraulics is not fast enough (even with the optimal PID setting). To check it, let us conduct dynamic analysis of the test setup, first as an open system.

The test setup may be idealized as shown in Fig. 1, where $u(t)$ is the load-point displacement of the test specimen, $v(t)$ is the displacement at the attachment of the grips (or fixture) to the loading frame, and $y(t)$ is the input from the electronic control, representing the prescribed load–displacement history (t = time). The effective mass of the machine frame is denoted as M, and the mass of the grips as m_g, including the mass of the specimen (which is, however, negligible in the case of composites). The mass and stiffness of the load cell are considered to be included in M and K_M.

To control the test, the controller of the machine sends a signal to the servo valve. The hydraulic pressure on the piston increases and the piston moves, but not immediately. The halftime, τ, of the hydraulics response delay, τ, which is of the order of 0.02 s (and is assumed to correspond to the optimized PID setting), may be modeled by a damper of viscosity constant

$$\eta = K_m \tau \tag{10}$$

Because the system can be considered incrementally linear, it will suffice to analyze the response to a sudden unit change of y, i.e., $y = H(t)$ where H denotes the Heaviside step function. Because only infinitely small increments are considered, the response may be considered to be linear and K_s to be constant, characterizing the steepest postpeak slope of the postpeak load displacement curve ($K_s < 0$). We also assume that no unloading would occur (because, for unloading, K_s would switch to a positive value).

The equations of motion can be derived from the Lagrange equations

$$\frac{\partial}{\partial t}\left(\frac{\partial L}{\partial \dot{v}}\right) - \frac{\partial L}{\partial v} + \frac{\partial \mathcal{D}}{\partial \dot{v}} = 0 \tag{11}$$

$$\frac{\partial}{\partial t}\left(\frac{\partial L}{\partial \dot{u}}\right) - \frac{\partial L}{\partial u} + \frac{\partial \mathcal{D}}{\partial \dot{u}} = 0 \tag{12}$$

$$\text{where} \quad L = T - V \tag{13}$$

$$T = \frac{1}{2} M\dot{v}^2 + \frac{1}{2} m_g \dot{u}^2 \tag{14}$$

$$V = \frac{1}{2} K_M (v-y)^2 + \frac{1}{2} K_g (v-u)^2 + \frac{1}{2} K_s u^2 \tag{15}$$

$$\mathcal{D} = \frac{1}{2} K_M \tau (\dot{v} - \dot{y})^2 \tag{16}$$

where the superior dots denote derivatives with respect to time t. Eqs. (11) and (12) yield the following equations of motion:

$$M\ddot{v} + K_M(v-y) + K_M \tau(\dot{v} - \dot{y}) + K_g(v-u) = 0 \tag{17}$$

$$m_g \ddot{u} + K_g(u-v) + K_s u = 0 \tag{18}$$

where $K_M \tau$ was substituted. While the system is nonlinear, the foregoing equations are linear. Therefore, u, v, and y should be regarded (similar to the derivation of Eq. 5) as small incremental displacements from an initial equilibrium state. If the incremental displacements are unstable (or uncontrollable), the actual nonlinear system is, too.

It is convenient to rewrite the equations of motion in the phase space by introducing new variables

$$x_1 = u, \quad x_2 = \dot{u}, \quad x_3 = v, \quad x_4 = \dot{v} \tag{19}$$

Substitution into the equations of motion gives a system of first-order ordinary linear differential equations in matrix form

$$\begin{Bmatrix} \dot{x}_1 \\ \dot{x}_2 \\ \dot{x}_3 \\ \dot{x}_4 \end{Bmatrix} = \begin{bmatrix} 0 & 1 & 0 & 0 \\ -\dfrac{K_g + K_s}{m_g} & 0 & -\dfrac{K_g}{m_g} & 0 \\ 0 & 0 & 0 & 1 \\ \dfrac{K_g}{M} & 0 & -\dfrac{K_M + K_g}{M} & -\dfrac{K_M \tau}{M} \end{bmatrix} \times \begin{Bmatrix} x_1 \\ x_2 \\ x_3 \\ x_4 \end{Bmatrix} + \begin{Bmatrix} 0 \\ 0 \\ 0 \\ \dfrac{K_M}{M} y + \dfrac{K_M \tau}{M} \dot{y} \end{Bmatrix} \tag{20}$$

The homogeneous part of this first-order matrix differential equation is satisfied by functions of the form $x_n = a_n e^{\lambda t}$ ($n = 1, 2, 3,$ and 4). Substitution into the homogeneous part of the foregoing matrix differential equation yields a homogeneous matrix algebraic equation for the column matrix of a_n. It has a nonzero solution if and only if λ is equal to the eigenvalues of the square matrix in Eq. (20). The solution is stable if and only if, for all the eigenvalues

$$\mathrm{Re}(\lambda) < 0 \tag{21}$$

For calculations, we consider first the aforementioned machine and test properties with the standard (light) grips. Then the following column matrix of eigenvalues is calculated:

$$\{\lambda\} = \begin{Bmatrix} 80.65 \\ -1.035 \times 10^4 \\ -77.17 \\ -53.87 \end{Bmatrix} \tag{22}$$

The presence of a positive eigenvalue, λ_1, indicates that, with the normal grips, the test of postpeak is unstable, which means that postpeak softening cannot be observed, as known from experience. Also note that the eigenvalues are real, which means that the stability loss is a divergence rather than flutter (oscillatory instability). Thus the static stability check in Eq. (3) is sufficient.

Second, consider the new grips of mass $m_g = 10\, m_{g0} = 9.419$ kg and stiffness $K_g = 10 K_{g0} = 2.6 \times 10^9$ N/m (Fig. 3). All the other parameters remain the same. Calculations yield the eigenvalue matrix (with $i^2 = -1$)

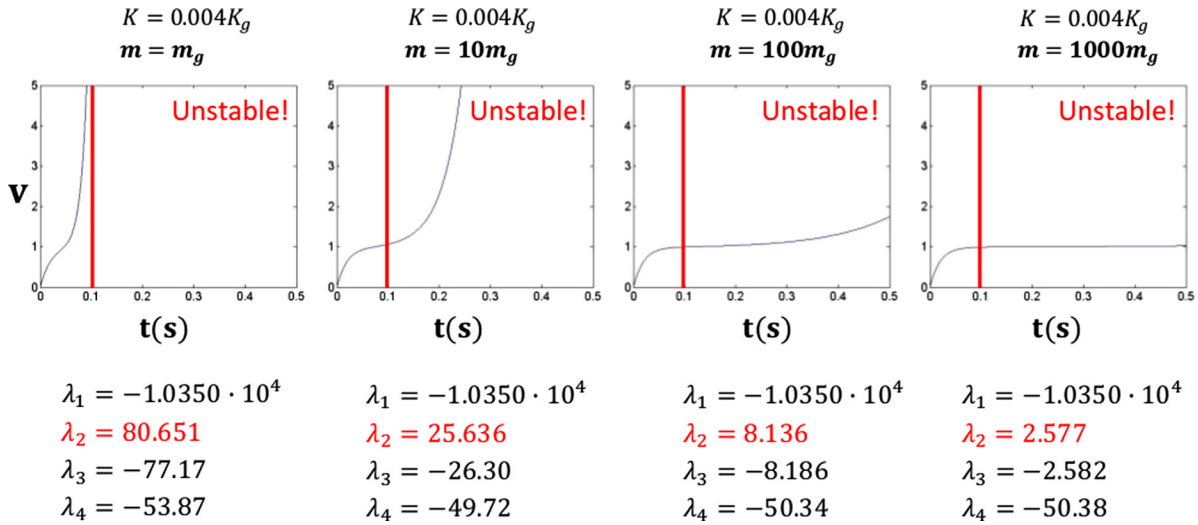

Fig. 4 Load-point control stability analysis for various values of grip mass, m_g

$$\{\lambda\} = \begin{Bmatrix} -15.78 + 4.52i \cdot 10^3 \\ -15.78 - 4.52i \cdot 10^3 \\ -1.032 \cdot 10^4 \\ -50.129 \end{Bmatrix} \tag{23}$$

All $\mathrm{Re}(\lambda)$ values are negative. So the specimen is stable, even under load-point control. This confirms the previous finding by static stability analysis, Eq. (4).

Adding Mass to Achieve CMOD Controllability With Soft Grips

Why has not the CMOD or CTOD control worked with the standard grips? Obviously, it would have to work if the response of the controls was infinitely fast. But with a hydraulic system this is impossible. The specimen accelerates fast in dynamic motion before the hydraulics can adjust the displacement.

Intuitively, the way to slow down the acceleration is to attach mass to the grips. So, consider the grip mass m_g to be increased to $\bar{m}_g = 10\,m_g, 100\,m_g$, and $1000\,m_g$, without increasing the grip stiffness. This leads to the sets of eigenvalues listed under the diagrams of Fig. 4. All of these sets include an eigenvalue with $\mathrm{Re}(\lambda) > 0$, which means the specimens are unstable—but unstable under controlled load-point displacement.

With a view of CMOD control, let us calculate the response of the system for input $y(t) = H(t)$ (Heaviside step function) under four initial conditions $u = \dot{u} = v = \dot{v} = 0$. The solution is obtained as a sum of the particular solution and a linear combination of four eigenvectors. The response curves of $u(t)$ are plotted in the four diagrams of Fig. 4. Note that, with increasing grip mass, the time at the onset of sharp exponential acceleration of displacement $u(t)$ (briefly "onset time") greatly increases.

To compare the onset time with the performance of the hydraulics, we plot in the figure vertical lines at time of 0.1 s, which is five times longer than the halftime of the hydraulics delay. We assume that by this time the CMOD control should be able to enforce the specified load-point displacement u with sufficient accuracy.

In the first diagram of Fig. 4, which corresponds to the standard (light) grips, the rise of exponential acceleration of $u(t)$ begins much before the critical time of 0.01 s. Obviously, the controls are too slow to prevent this acceleration, which inevitably leads to sudden failure. However, as seen in the third diagram, the grip mass of $100\,m_g$ postpones the acceleration well beyond 0.1 s, and here the hydraulics controlled by the CMOD should evidently be able to impose the required load-point displacement.

According to the second diagram for $10\,m_g$, it seems the exponential acceleration could also be prevented, but better informed analysis of the hydraulic system and trial testing may be needed. And the fourth diagram, for $1000\,m_g$, is obviously an overkill.

Stability Analysis of Closed-Loop PID System Under CMOD Control

The closed-loop control of the modern testing machines is based on a proportional-integrative-differential (PID) signal of the error $w_D - w$ where w_D = desired crack mouth opening displacement (CMOD) and w = CMOD measured by the extensometer; see the schematic of the control loop in Fig. 5.

Combining Eqs. (6) and (7) and integrating over a small time interval with constant tangential stiffnesses, one gets $w = C_{sc}/C_s u$ where $u(0) = w(0) = 0$ may be assumed. Accordingly, the equations of motion of the system may be written as

$$\begin{cases} m\ddot{u} + K_g(u - v) + K_s(u) = 0 \\ M\ddot{v} + K_M\left[\zeta(v,u,y) + \tau\dot{\zeta}(v,u,y)\right] + K_g(v - u) = 0 \\ \zeta(v,u,y) = v - y + \left(\dfrac{C_{sc}}{C_s}u - w_D\right)K_p + \left(\dfrac{C_{sc}}{C_s}\dot{u} - \dot{w}_D\right)K_D \\ \qquad + K_I\displaystyle\int_0^t \left(\frac{C_{sc}}{C_s}u - w_D\right)\mathrm{d}t' \end{cases} \tag{24}$$

where K_p is the proportional gain of the PID control and K_g is the stiffness of the grips. Introducing the transformation:

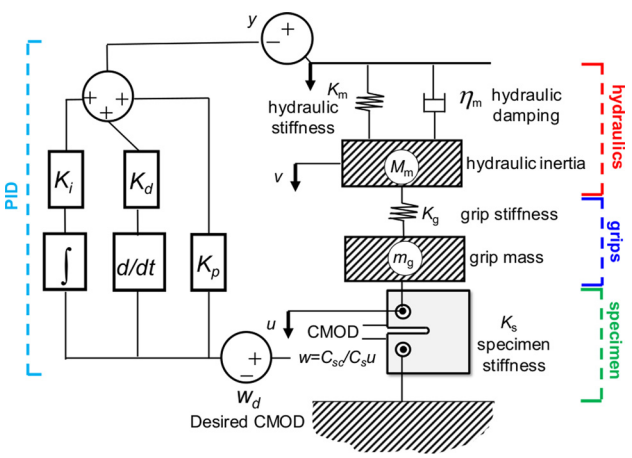

Fig. 5 Schematic of machine and testing setup including the PID control

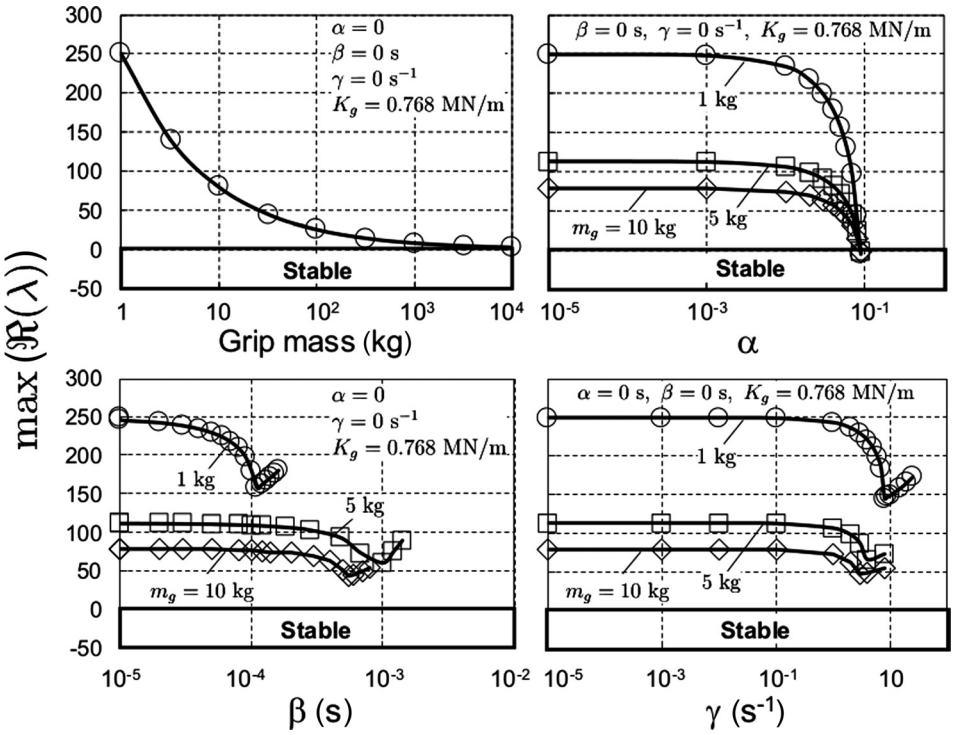

Fig. 6 Effect of grip mass on (*a*) open system, (*b*) proportional control, (*c*) differential control, and (*d*) integrative control

$$x_1 = u, \quad x_2 = \dot{u}, \quad x_3 = v, \quad x_4 = \dot{v}, \quad x_5 = \int x_1 \mathrm{d}t \tag{25}$$

the system of equations becomes

$$\begin{cases} \dot{x}_1 = x_2 \\ \dot{x}_2 = -\dfrac{1}{m}\left[K_g(x_1 - x_3) + K_s(x_1)\right] \\ \dot{x}_3 = x_4 \\ \dot{x}_4 = -\dfrac{1}{M}\left\{K_M[x_3 + \alpha x_1 + \beta x_2 + \gamma x_5]\right. \\ \qquad + K_M\tau\left[x_4 + \alpha x_2 - \dfrac{\beta}{m}K_g(x_1 - x_3) - \dfrac{K_s}{m}\beta x_1 + \gamma x_1\right] \\ \qquad \left. + K_g(x_3 - x_1)\right\} - K_M\chi(y, w_D) \\ \dot{x}_5 = x_1 \end{cases} \tag{26}$$

where $\alpha = (C_{sc}/C_s)K_p$, $\beta = (C_{sc}/C_s)K_d$, $\gamma = (C_{sc}/C_s)K_i$ and

$$\chi = \left[y - \alpha w_D - \beta \dot{w}_D - \gamma \int w_D \mathrm{d}t' + \tau(y - \alpha \dot{w}_D - \beta \ddot{w}_D - \gamma w_D)\right. \tag{27}$$

The foregoing system is stable if the linearized system is stable (see Refs. [6–8], Chap. 3). Stability requires that all the eigenvalues λ of the matrix of Eq. (26), given below, be negative

$$\begin{bmatrix} -\lambda & 1 & 0 & 0 & 0 \\ -\dfrac{1}{m}\left(K_g + \dfrac{\partial K_s}{\partial x_1}\right) & -\lambda & \dfrac{K_g}{m} & 0 & 0 \\ 0 & 0 & -\lambda & 1 & 0 \\ R_1 & -\dfrac{\beta K_M}{M} & R_2 & -\dfrac{K_M\tau}{M} & -\dfrac{Km\gamma}{M} - \lambda \\ 1 & 0 & 0 & 0 & -\lambda \end{bmatrix} \tag{28}$$

where $R_1 = \dfrac{K_g - \alpha K_M}{M} + \dfrac{K_M\tau}{M}\left[\gamma + \beta\dfrac{\partial K_s/\partial x_1 + K_g}{m}\right]$ (29)

$$R_2 = -\frac{K_M + K_g}{M} + \frac{\beta\tau K_g K_M}{mM} \tag{30}$$

The calculation results shown in Figs. 6 and 7 show the effects of the mass and thickness of the grips, respectively. The stiffness has a big effect on stability but, at first surprisingly, the mass has none. That calls for discussion from a different viewpoint—controllability.

Controllability Versus Stability

According to Lyapunov's definition of stability (see Refs. [6–8], Sec. 3.5], the response $x_i(t)$ of a dynamic system with initial state x_i^0 is *stable* if, for an arbitrarily small positive number ϵ, there exists a positive number δ such that the response to any change of the initial state x_i^0 smaller than δ will *never* deviate from $x_i(t)$ by more than ϵ. But, in a closed system with active input $y(t)$, what matters is the controllability.

A state x_i' is controllable at time t' if there exists an input $y(t)$ that transfers the state $x_i(t)$ from x_i' to the specified state x_i^* within some finite time interval Δt. If this is true for all t', the system is controllable. Generally, a stable system is controllable, but a system can be controllable even if it is unstable (note that modern aircraft fly with long wings that are unstable but controllable). While, as we showed, the mass has no effect on stability, it has a big effect on controllability, as is obvious from Fig. 4. The following five observations can be made:

(1) Although increasing the mass of the grips decreases the most critical eigenvalue (a tenfold increase of m_g reduces the most critical eigenvalue by 70%), stability can be reached only with infinite mass.
(2) The proportional gain of the PID control, K_p, is the one having the greatest effect on stability. Increasing the mass

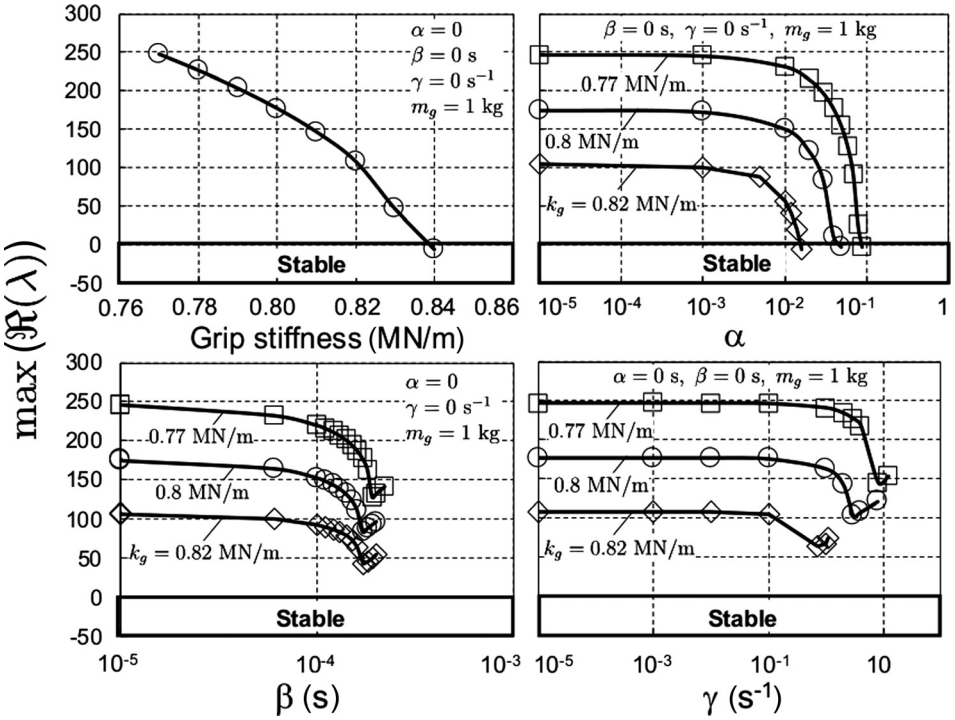

Fig. 7 Effect of grip stiffness on (*a*) open system, (*b*) proportional control, (*c*) differential control, and (*d*) integrative control

of the grips does not increase the range of values of K_p leading to stability.

(3) The derivative and integrative gains play a secondary role in stability compared to the proportional gain. Increasing m_g does not have a very significant effect on these parameters.

(4) A huge effect of grip stiffness stability (exemplified here by stability attainment, even without CMOD control, with a mere 9% stiffness increase) is not the only effect of grip stiffness, K_g. A further effect is a significant contribution to the proportional gain. Increasing the stiffness by 2% reduces the minimum value of K_p leading to stability by 80%, thus making the test control much easier.

(5) On the other hand, the grip stiffness does not have a strong effect on the integrative and derivative gains.

Experimental Verification of Stable Postpeak Softening of Compact Tension Specimens

Figure 3 shows the compact-tension fracture specimen of woven carbon-epoxy specimens used to study the postpeak behavior and determine the fracture energy G_f of the material and provides a general view of the test setup in an MTS testing machine.

Figure 8 shows the photos of the current standard grips (on the left) and of the proposed massive grips (on the right) that successfully stabilized the postpeak.

Figure 9 demonstrates several stable postpeak load-deflection diagrams measured with the proposed stiff grips on the compact-tension specimens.

Agreement of G_f From Size Effect Tests With G_f From the Area Under Complete Load-Displacement Curve

The area A under the complete stable load–displacement curve of the fracture specimen allows estimating the fracture energy, G_f, of the material; $G_f = A/Lb$ where l = length of the broken ligament and b = specimen thickness (provided that the energy dissipation outside the fracture is negligible.

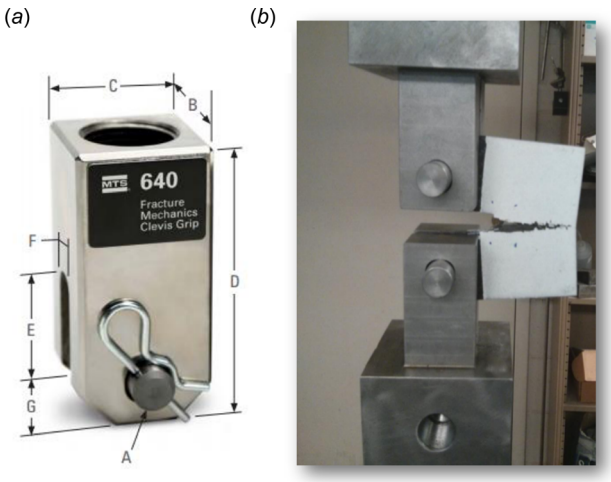

Fig. 8 (*a*) Example of MTS standard grip and (*b*) newly designed grips of increased stiffness and mass

Another, easier, way to determine the fracture energy is the size effect method [9]. For this purpose, it was more convenient to use tensile tests of geometrically similar edge-notched strip specimens of three different sizes, as shown in Fig. 10. This method uses only the maximum loads and the postpeak softening is not needed. So it sufficed to conduct the tests with the standard grips, even though the specimen failed right after the peak load. The fracture energies obtained from the size effect and from the postpeak were, respectively

$$\begin{aligned} &\text{from size effect:}\quad G_f = 73.7\ \text{N/m}\ \text{ and} \\ &\text{from postpeak:}\quad G_f = 78\ \text{N/m} \end{aligned} \tag{31}$$

It is remarkable that the difference between these two values is only 5.8%. Besides it is logical that the size effect gives the

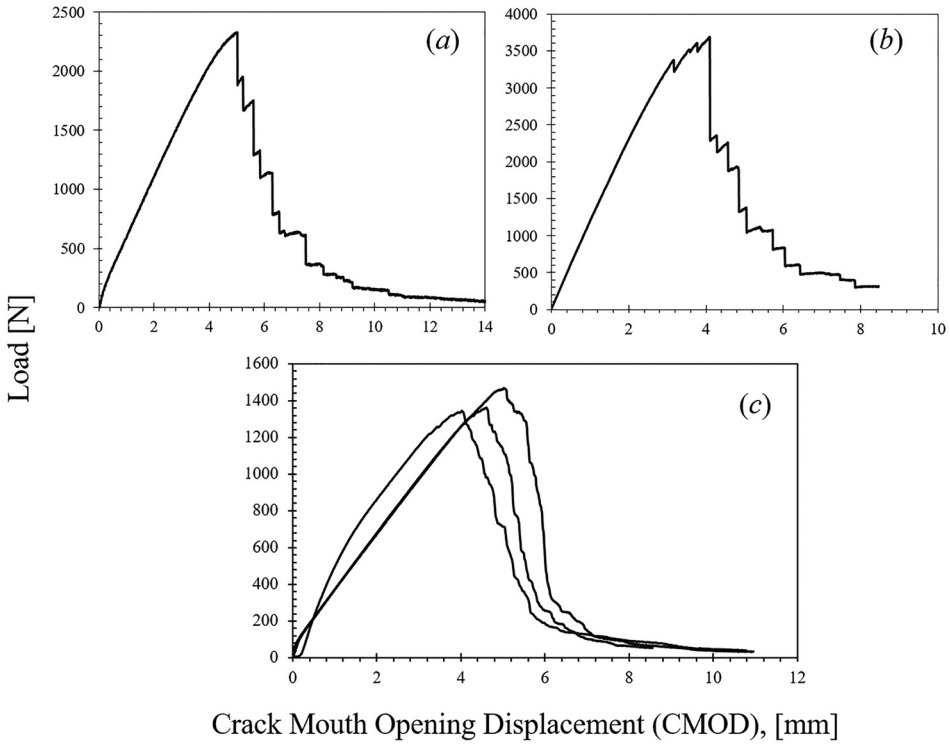

Fig. 9 Examples of typical stable load-displacement curves obtained with the newly designed grips for carbon fiber woven composites (*a*) and (*b*) and for glass fiber textile composites (*c*)

smaller of the two values because the size effect method does not capture the area under the tail of the softening curve.

Nonexistence of Snapback and of Conflict With Size Effect

Because it was impossible to observe postpeak softening, it has been believed for decades that the fracture specimens of composites exhibit a severe snapback. Thanks to stiffening the grips, we now see that this view was incorrect.

The misconception of snapback further shed false doubts on the applicability of fracture mechanics to fiber composites. The area under the supposed snapback curve, which must in any case be smaller than the area under a load-deflection curve with sudden vertical load drop from the peak-load point, gave fracture energy much smaller than that deduced from the size effect, or from the measured drop of complementary energy of test specimen.

For some investigators, this severe mismatch was another reason to consider quasibrittle cohesive fracture mechanics as inapplicable to fiber composites. Now we see that this interpretation was mistaken.

The present analytical and experimental results, and especially Eq. (31), prove that fracture mechanics is perfectly applicable to fiber composites.

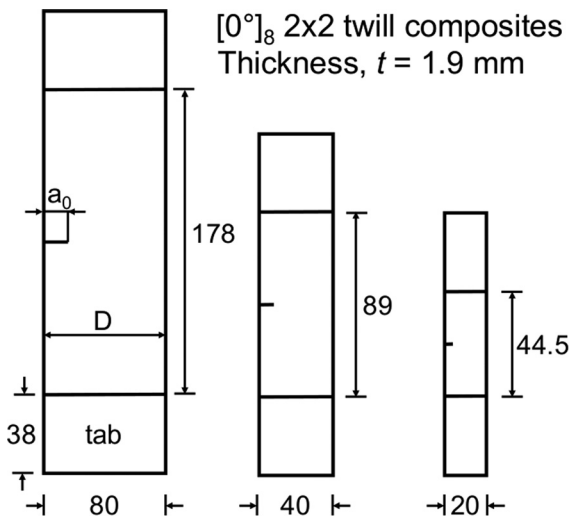

Fig. 10 Geometry of single edge notched tension (SENT) specimens used (units: mm)

Why the Postpeak in Delamination Fracture Tests Has Been Stable?

To determine the delamination fracture energy of the same carbon composite, the ASTM standard test specimen [13] was used. In these tests, the gradual postpeak softening was stable, even with the standard grips. Why? The explanation is that the delamination specimens are much softer than the compact tension specimens. If $|K_s|$ is small enough, K_t ceases to be negative since the first term in Eq. (2) is always positive. We see that the required stiffness of the grips increases with the stiffness of the fracture specimen.

Conclusions

(1) The specimen grips (or fixtures) of the contemporary hydraulic servo-controlled testing machines do not have sufficient stiffness and mass to enable stable measurement of postpeak softening of fracture specimens of very strong and very light materials such as fiber composites.
(2) By stability analysis based on the second law of thermodynamics, it is shown that the cause of pervasive failure to observe postpeak softening during the past half century of composites testing has been the instability due to insufficient stiffness and mass of the specimen grips.
(3) Based on static stability analysis of the test setup, it is proposed to use grips that are stiffer by about two orders of

magnitude. Calculations show that, in this way, stability is achieved.

(4) Experiments on compact-tension fracture specimens of woven fiber-polymer composites confirm the observability of stable postpeak, not only for the CMOD control but also for the load-point displacement control.
(5) The grip stiffness required for stability and controllability increases with the stiffness of the fracture specimen.
(6) Calculations of the eigenvalues of the equations of motion of the test setup confirm that the grip stiffness has a huge effect on static as well as dynamic stability, making the PID control much easier.
(7) Calculations also indicate a large effect of the increase of mass of the grips on controllability of the postpeak response under PID control, although the effect on stability is nil.
(8) Calculations further indicate that, if a sufficient mass is rigidly attached to the existing soft grips, the postpeak response under PID control of the CMOD should become controllable (this is a theoretical inference that still remains to be verified by experiment).
(9) The present stability analysis also explains why the switch in the 1960 s to far stiffer testing frames sufficed to stabilize the postpeak softening in concrete and rocks, but not in composites. The specimens of concrete and rock are generally far more massive and their attachments (consisting of flat contacts, glued in the case of tension) have naturally been far stiffer than those used for fiber composites.
(10) The previous view that the impossibility of measuring postpeak softening necessarily implied a severe snapback is not correct. In the usual compact-tension specimens, there is no snapback.
(11) The previous inference that the smallness of the area under the supposed snapback curve conflicted with G_f measured from the size effect or from the energy release was thought to invalidate fracture mechanics. This inference was false.
(12) The present results prove that quasibrittle fracture mechanics, with a finite fracture process zone and a transitional size effect, is perfectly applicable to fiber composites.
(13) The present results also prove that the previously widespread use of plasticity-based failure envelopes in terms of stress or strain has not been correct.

Acknowledgment

Partial funding obtained from the NSF under Grant No. CMMI-1439960, from the ARO under Grant No. W911NF-15-1-0240, and from the USCAR consortium (through Ford Motor Co.) under Grant No. 13-2856-AMR/DE-EF0005661, all to Northwestern University, is gratefully acknowledged. Partial funding for the theoretical analysis of fracturing of quasibrittle materials in general has also been obtained under ARO Grant W011NF-15-1-0240 to Northwestern University.

Appendix: Details of Experiments

Materials

Experiments were conducted on woven composite specimens manufactured by compression molding. A bisphenol A diglycidyl ether based epoxy resin was chosen as polymer matrix whereas the reinforcement was provided by a twill 2×2 fabric made of carbon fibers. The material was characterized following the ASTM standard procedures [27] for testing under compact tension. The material was a $[0\,\text{deg}]_8$ lay-up with a constant thickness of approximately 1.8 mm.

Further experiments were conducted on fiberglass reinforced polyester (FRP) composite, with the thickness of about 10 mm.

Specimen Characteristics

The modified compact tension (CT) specimen geometry was recently developed at Northwestern University research group to produce stable crack growth so that the composite damage zone could be investigated. Initially, a 2 mm wide notch was created by using diamond band saw. Then, the notch was extended by using artistic wire saw in order to create a shape notch tip of 0.2 mm in radius. The CT specimen with a sharp notch tip is stable under displacement control and is large enough so that the boundaries do not greatly affect the damage zone size or shape.

The specimen was loaded in tension through pins located above and below the notch. It was found that the pin holes cannot be made using steel drill bits because the carbon fiber is harder than the steel from which the drill is made. To avoid damage due to fiber tear-out and delamination around the holes caused by steel drill bits, abrasive cutting with tungsten grinding bits for nonmetals was used to create these holes. The specimen thickness of 5.4 mm sufficed to prevent buckling of the woven composite material.

Furthermore, intralaminar size effect tests were conducted on single-edge-notched tension (SENT) specimens (see Fig. 10), using a $[0\,\text{deg}]_8$ lay-up with a constant thickness of approximately 1.9 mm. The SENT specimens were preferred to double-edge notched tension (DENT) specimens because in these specimens the response path bifurcates such that only one of the two cracks can propagate, causing asymmetric response [28].

SENT specimens of three sizes (three for each size), geometrically scaled in two-dimensions in the ratio 1:2:4, were tested. The specimen lengths, $L + 2L_t$, were respectively, 120.5, 165.0, 254.0 mm; the gauge lengths 44.5, 89.0, 178.0 mm; the widths 20, 40, 80 mm; and the notch lengths 4, 8, 16 mm. The thickness was 1.9 mm, and the tab length $L_t = 38$ mm, the same for all the sizes. The glass-epoxy tabs, for gripping purposes, were not scaled because they have no appreciable effect on the stored energy release and because fracture always occurs away from the grips.

The first half of the notch of SENT specimens was cut by means of a diamond-coated bend saw which provided a width of roughly 1 mm. The second half of the notch was cut by a diamond-coated miniature blade, thanks to which a notch width of only 0.2 mm was achieved in all cases. Accordingly, the resulting crack tip radius was 0.1 mm, about 70 times smaller than the size of a representative unit cell (RUC) of the material.

The top surface of all the SENT specimens investigated was treated to allow digital image correlation (DIC) analysis. A thin layer of white paint was deposited on a $D \times D$ area embedding the crack. Then, black speckles of average size 0.01 mm were spray-painted on the surface after drying.

Testing

The compact tension (CT) test setup is shown in Fig. 3. A universal testing machine (of MTS) was used to load the CT specimens at the rate of 1 mm/min. Tensile loading was applied through 20 mm diameter pins inserted through the holes shown in Fig. 1(*a*). An extensometer was attached to the specimens to measure the pin opening displacement (POD). The load cell signal and the extensometer signal were output and recorded.

Size Effect Tests on Single Edge-Notched Tension (SENT) Specimens

After the completion of the experiments, the load and displacement data were analyzed. Figure 11 shows, for the various sizes, the typical load–displacement plots reported. It is worth noting that, for the largest specimen size, these curves are almost linear up to failure, which is an indication of pronounced brittle behavior.

Right after reaching the peak load, the specimens used for size effect became unstable for all the sizes and failed dynamically. This was no problem since the size effect analysis does not require postpeak (note that stiff grips cannot stabilize these specimens

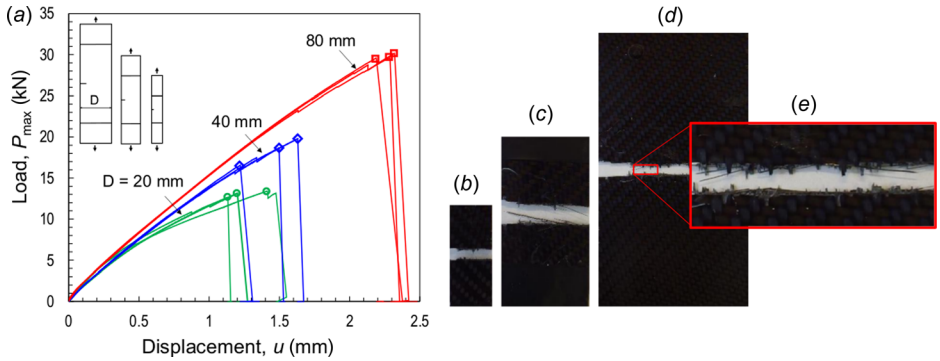

Fig. 11 (*a*) Typical load-displacement curves of $[0deg]_8$ geometrically scaled SENT specimens of various sizes, showing decreasing nonlinearity at increasing specimen size. Typical failure patterns of SENT specimens for width (*b*) $D = 20$ mm, (*c*) $D = 40$ mm, and (*d*) $D = 80$ mm. (*e*) Magnification of fracture surface for the large size specimen showing extensive tow failure and pull out (the postpeak is here dynamic; note that, for size effect testing, a stable postpeak control is not needed).

because the specimen itself is too soft and stores too much energy). The failed specimens showed microcracks within the layers, and tow breakage or pull-out. Delamination between the layers occurred before the peak load.

Note that, according to strength-based criteria (e.g., Tsai and Wu [1]), the nominal strength would not depend on the structure size. However, Table 3 does show a significant decrease of σ_N with an increasing characteristic size of the specimen, which proves the strength-based failure criteria to be incorrect.

From the size effect results, the initial fracture energy was obtained as $G_f = 73.7$ N/mm.

Compact Tension Test Results

Figure 9 gives the load versus pin opening displacement (POD) curves of all the tested specimens. For woven composite specimens, it can be seen that the load versus POD curves are approximately linear up to the first load drop. After that, the crack progresses in a series of small jumps that cause further load drops.

In contrast, the FRP specimens showed a large degree of nonlinearity in the load versus POD curves. Figures 9(*a*)–9(*c*) show failure modes typical of woven composites and FRP composite specimens. The failure of woven composite is characterized by development of fiber breakage along the center line of the specimen toward the back. A small amount of splitting can be observed on either side of the fiber breaks, which caused flaking of the paint for the digital image correlation (DIC).

From the load versus POD curves (Fig. 9), the fracture energy of the composites can be estimated as [9]:

$$G_f = \frac{W}{b\, l_l} \tag{A1}$$

where G_f = fracture energy, W = area under the load displacement curve, b = thickness of the specimen, and l_l = ligament length. The calculated fracture energies for woven composites are 76.34 N/mm and 79.74 N/mm for specimens 1 and 2, respectively. These results are very close to the fracture energy calculated from the size effect using the size effect test (since the size effect method gives the fracture energy corresponding only to the area under the initial tangent to the cohesive stress-displacement law, it appears that this law should not have a long tail of small slope). The fracture energies of FRP composites deduced from the size effect were 15.97 N/mm, 16.47 N/mm, and 18.88 N/mm for specimens 1, 2, and 3, respectively.

References

[1] Tsai, S. W., and Wu, E. M. A., 1972, "General Theory of Strength for Anisotropic Materials," J. Compos. Mater., **5**(1), pp. 58–80.

[2] Hinton, M. J., and Soden, P. D., 1998, "Predicting Failure in Composite Laminates: The Background to the Exercise," Compos. Sci. Technol. J., **58**(7), pp. 1001–1010.

[3] Soden, P. D., Hinton, M. J., and Kaddour, A. S., 1998, "A Comparison of the Predictive Capabilities of Current Failure Theories for Composite Laminates," Compos. Sci. Technol. J., **58**(7), pp. 1225–1254.

[4] Hinton, M. J., Kaddour, A. S., and Soden, P. D., 2002, "A Comparison of the Predictive Capabilities of Current Failure Theories for Composite Laminates, Judged Against Experimental Evidence," Compos. Sci. Technol. J., **62**(12–13), pp. 1725–1797.

[5] Bažant, Z. P., 1984, "Size Effect in Blunt Fracture: Concrete, Rock, Metal," J. Eng. Mech. ASCE, **110**(4), pp. 518–535.

[6] Bažant, Z. P., and Cedolin, L., 1991, *Stability of Structures: Elastic, Inelastic, Fracture and Damage Theories*, Oxford University Press, New York.

[7] Bažant, Z. P., and Cedolin, L., 2003, *Stability of Structures: Elastic, Inelastic, Fracture and Damage Theories*, 2nd, ed., Dover Publication, New York.

[8] Bažant, Z. P., and Cedolin, L., 2010, *Stability of Structures: Elastic, Inelastic, Fracture and Damage Theories*, 3rd, ed., World Scientific, Hackensack, NJ.

[9] Bažant, Z. P., and Planas, J., 1998, *Fracture and Size Effect in Concrete and Other Quasibrittle Material*, CRC Press, Boca Raton, FL.

[10] Bažant, Z. P., Daniel, I. M., and Li, Z., 1996, "Size Effect and Fracture Characteristics of Composite Laminates," ASME J. Eng. Mater. Technol., **118**(3), pp. 317–324.

[11] Green, B. G., Wisnom, M. R., and Hallet, S. R., 2007, "An Experimental Investigation Into the Tensile Strength Scaling of Notched Composites," Composites—Part A, **38**(3), pp. 867–878.

[12] Bažant, Z. P., 1976, "Instability, Ductility and Size Effect in Strain-Softening Concrete," J. Eng. Mech. Div. ASCE, **102**(2), pp. 331–344.

[13] ASTM, 2007, "Standard Test Method for Mode I Interlaminar Fracture Toughness of Unidirectional Fiber-Reinforced Polymer Matrix Composites," ASTM International, West Conshohocken, PA, Standard No. ASTM D5528.

[14] Salviato, M., Kirane, K., Ashari, S. E., Bažant, Z. P., and Cusatis, G., 2016, "Experimental and Numerical Investigation of Intra-Laminar Energy Dissipation and Size Effect in Two-Dimensional Textile Composites," Compos. Sci. Technol., (in press).

[15] Bažant, Z. P., 1999, "Size Effect on Structural Strength: A Review," Archive Appl. Mech., **69**(9), pp. 703–725.

[16] Bažant, Z. P., Kim, J.-J. H., Daniel, I. M., Becq-Giraudon, E., and Zi, G., 1999, "Size Effect on Compression Strength of Fiber Composites Failing by Kink Band Propagation," Int. J. Fract., **95**, pp. 103–141.

[17] Bažant, Z. P., Zhou, Y., Novak, D., and Daniel, I. M., 2004, "Size Effect on Flexural Strength of Fiber-Composite Laminates," ASME J. Eng. Mater. Technol., **126**(1), pp. 29–37.

[18] Salviato, M., Kirane, K., Ashari, S., Bažant, Z. P., and Cusatis, G., 2016, "Experimental and Numerical Investigation of Intra-Laminar Energy Dissipation and Size Effect in Two-Dimensional Textile Composites," Cornell University Library, Ithaca, NY, Report No. SEGIM 16-05/707E.

[19] Bažant, Z. P., Chau, V. T., Cusatis, G., and Salviato, M., 2016, "Direct Testing of Gradual Postpeak Softening of Notched Specimens of Fiber Composites Stabilized by Enhanced Stiffness and Mass," Cornell University Library, Ithaca, NY, Report No. 16-07/d.

[20] Rüsch, H., and Hilsdorf, H., 1963, "Deformation Characteristics of Concrete Under Axial Tension," Voruntersuchungen Bericht (preliminary report) Report No. 44.

[21] Hughes, B. P., and Chapman, G. P., 1966, "The Complete Stress-Strain Curve for Concrete in Direct Tension," RILEM Bull. (Paris), **30**, pp. 95–97.

[22] Evans, R. H., and Marathe, M. S., 1968, "Microcracking and Stress-Strain Curves in Concrete for Tension," Mater. Struct., **1**(1), pp. 61–64.

[23] Heilmann, H. G., Hilsdorf, H., and Finsterwalder, K., 1969, "Festigkeit und Verformung von Beton unter Zugspannungen," Deutscher Ausschu s für Stahlabeton, Heft 203.
[24] Wawersik, W. R., and Fairhurst, C., 1970, "A Study of Brittle Rock Fracture in Laboratory Compression Experiments," Int. J. Rock Mech. Min. Sci., **7**(5), pp. 561–575.
[25] Hudson, J. A., Brown, E. T., and Fairhurst, C., 1971, "Optimizing the Control of Rock Failure in Servo-Controlled Laboratory Tests," Rock Mech., **3**(4), pp. 217–224.
[26] Fairhurst, C., private communication on June 23, 2016 to Z. P. Bazant of the Photo of the First MTS Stiff Machine Built in 1968 in Collaboration With Fairhurt and Wawerskik.
[27] ASTM, 1999, "Standard Test Methods for Plane-Strain Fracture Toughness and Strain Energy Release Rate of Plastic Materials," ASTM International, West Conshohocken, PA, Standard No. ASTM D5045.
[28] Bažant, Z. P., and Tabbara, M. R., 1992, "Bifurcation and Stability of Structures With Interacting Propagating Cracks," Int. J. Fract., **53**(3), pp. 273–289.